Nernst effect in the electron-doped cuprate superconductor $La_{2-x}Ce_xCuO_4$

P. R. Mandal, Tarapada Sarkar, J. S. Higgins, and Richard L. Greene[*]

Center for Nanophysics & Advanced Materials and Department of Physics, University of Maryland, College Park, Maryland 20742, USA

We report a systematic study of the Nernst effect in films of the electron-doped cuprate superconductor $La_{2-x}Ce_xCuO_4$ as a function of temperature and magnetic field (up to 14 T) over a range of doping from underdoped ($x = 0.08$) to overdoped ($x = 0.16$). We have determined the characteristic field scale H_{C2}^* of superconducting fluctuation which is found to track the domelike dependence of superconductivity (T_C). The fall of H_{C2}^* and T_C with underdoping is most likely due to the onset of long-range antiferromagnetic order. We also report the temperature onset, T_{onset}, of superconducting fluctuations above T_C. For optimally doped $x = 0.11$ T_{onset} ($\cong 39$ K) is high compared to T_C (26 K). For higher doping T_{onset} decreases and tends to zero along with the critical temperature at the end of the superconducting dome. The superconducting gap closely tracks H_{C2}^* measured from the temperature- and field-dependent Nernst signal.

I. INTRODUCTION

The nature of the normal state and the origin of the high-T_C superconductor (HTSC) in the cuprates is still a major unsolved problem. In the hole-doped cuprates a mysterious "pseudogap" is found, whose origin and relation to the HTSC is still not understood. Some early Nernst effect experiments [1] on underdoped p-type cuprates suggested that there is a significant temperature range above T_C where superconductivity (SC) fluctuations exist. This was supported by theory [2] and other experiments [3,4]. But, recently, the early interpretation of the Nernst effect has been questioned [5] and a much smaller temperature range of fluctuations has been proposed. Therefore, the issue of the range of SC fluctuations and their relation to the onset of the pseudogap in p-type cuprates is still controversial.

The electron-doped cuprates have a much simpler phase diagram with no p-type pseudogap. Prior Nernst effect experiments on n-type cuprates are basically in agreement that SC fluctuations occur over a rather narrow T range above T_C at all doping [1]. Surprisingly, a rather large normal-state (quasiparticle) Nernst effect was observed [6] in the overdoped regime where one might expect a small effect because only hole carriers dominate the transport properties there (i.e., large holelike Fermi surface). Stated another way, the Fermi surface reconstruction (FSR) in the n-type cuprates does not appear to impact the normal-state Nernst effect in any dramatic way, whereas the Hall effect and thermopower show large changes at the FSR doping [6,7].

In this paper we present Nernst effect experiments on another n-type cuprate, $La_{2-x}Ce_xCuO_4$ (LCCO). This research is motivated by the fact that LCCO can be doped over a wider range than other n-type cuprates. This allows us to examine the Nernst effect at doping throughout the SC dome including the FSR doping and to determine the temperature range of SC fluctuations over the entire SC dome.

The generation of a transverse electric field by a longitudinal thermal gradient and a perpendicular magnetic field, the Nernst effect, has attracted considerable attention in the cuprates due to observation of a large Nernst signal in the normal state. The Nernst effect is large in the superconducting state due to vortex motion but the normal-state quasiparticle contribution is usually small (except in two-band materials). The surprisingly large Nernst signal well above T_C in the underdoped p-type cuprates was attributed to SC phase fluctuations and vortexlike excitations [8,1]. The basic assumption of this interpretation was that the usual SC Gaussian amplitude fluctuations have a weak contribution to the Nernst signal above T_C. But, in 2006 Pourret *et al.* showed the existence of fluctuating Cooper pairs up to a high temperature ($T \approx 30 \times T_C$) and higher magnetic field ($H \approx 4 \times H_{C2}$) for a conventional superconductor Nb_xSi_{1-x} [9,10]. For Nb_xSi_{1-x} and another amorphous superconductor, InO_x, it was found that the fluctuations were in quantitative agreement with Gaussian fluctuations theory for a two-dimensional (2D) dirty superconductor [2]. The theory was restricted to low magnetic fields in the vicinity of the critical temperature. Later Michaeli and Finkel'stein developed theoretical calculations which explained quantitatively the experimental data of Nb_xSi_{1-x} at temperature much higher than the critical temperature and at magnetic field much higher than the upper critical field [11]. Still later, Taillefer and his collaborators [5,12] studied the Nernst effect in the hole-doped cuprate $La_{1.8-x}Eu_{0.2}Sr_xCuO_4$ and the electron-doped cuprate $Pr_{2-x}Ce_xCuO_4$ and concluded that quasiparticles and Gaussian fluctuations could explain the Nernst signal above T_C in the underdoped as well as the overdoped region. Moreover, the temperature range of these fluctuations in the normal state was much smaller than suggested by the work of Wang *et al.* [1].

There have been several prior Nernst effect experiments in different electron-doped cuprates. In 2003 Balci *et al.* [13] observed a large normal-state Nernst signal in $Pr_{2-x}Ce_xCuO_4$ (PCCO) films with Ce concentration varied around the optimal doping, which was in agreement with previous results in

─────────
*rickg@umd.edu

$Nd_{2-x}Ce_xCuO_4$ (NCCO) where the results were interpreted as the evidence for the existence of two-carrier transport [14]. In 2007 Li and Greene reported a systematic study of the normal-state Nernst effect in PCCO over a wide range of Ce concentration to investigate the transport properties in the very underdoped and overdoped region [6]. The surprisingly large Nernst signal observed in overdoped and lightly underdoped PCCO is of uncertain origin but could be explained by a two-band model. Recently Tafti *et al.* measured the Nernst signal in PCCO at four concentrations, from underdoped ($x = 0.13$) to overdoped ($x = 0.17$), for a wide range of temperatures above the critical temperature and showed that the data are quantitatively consistent with the theory of Gaussian superconducting fluctuations [12].

The detailed studies of the Nernst effect in electron-doped cuprates over a wide range of Ce concentration are important in order to understand the transport properties in the very underdoped or overdoped regimes. In this paper we study the vortex Nernst effect and superconducting fluctuations in the films of the electron-doped cuprate superconductor $La_{2-x}Ce_xCuO_4$ (LCCO) for both sides of the dome. The major advantage of using LCCO films is that we can study the Nernst effect up to the Fermi liquid regime, i.e., the more overdoped side ($x = 0.21$). Here we have studied how the SC fluctuations vary from the underdoped to the overdoped regime. Since optimal doping (0.11) [15] and the doping where the Fermi surface reconstruction occurs (0.14) are different, we can study the impact of the Fermi surface reconstruction on the Nernst effect. Another advantage is that a very low magnetic field of 14 T is enough to supress the superconducting fluctuations for LCCO films. We have found that the Nernst signal follows the Gaussian fluctuation theory for underdoped, optimally doped, and overdoped samples above the critical temperature, which is consistent with the previous results found in PCCO [12]. Also from our measurements we have determined Ce concentration dependence of the upper critical field H_{C2}^*, which characterizes the strength of the superconductivity. We found that H_{C2}^* exactly tracks the T_C dome. We also determined the extent of the SC fluctuation region above T_C for all doping.

II. EXPERIMENTAL DETAILS

The measurements have been performed on $La_{2-x}Ce_xCuO_4$ thin films for underdoped ($x = 0.08$), optimally doped ($x = 0.11$), and overdoped ($x = 0.13, 0.14, 0.15,$ and 0.16) compositions. The thin films were fabricated on (100) $SrTiO_3$ (10×5 mm^2) substrates by a pulsed laser deposition technique utilizing a KrF excimer laser [6]. The thickness of the samples used for this study is between 150 and 200 nm. The Nernst effect has been measured using a one-heater–two-thermometer technique. One end of the sample is attached to a copper block with a mechanical clamp and other end is left free. On the free end a small chip resistor heater is attached and two tiny Lakeshore Cernox thermometers are on the two ends of the sample to monitor the temperature gradient (0.7–1 K) continuously. The Nernst voltage measurements have been performed using a Keithley 2001 multimeter with sensitivity of several nanovolts by applying a magnetic field between 14 and -14 T in a Physical Property Measurement System (PPMS). The measurements were done under high vacuum

and the magnetic field has been applied perpendicular to the *ab* plane. The sample temperature is taken as the average of hot and cold end temperatures. The final Nernst signal is obtained by subtracting the Nernst data at negative field from the Nernst data at positive field to eliminate any possible contribution from the Seebeck effect.

III. RESULTS

A. In-plane resistivity

A standard four-probe method has been used to measure the resistivity ρ of LCCO thin films at zero magnetic field. To understand the superconducting phase diagram we have studied the resistivity at zero field and higher magnetic field and the normal-state Hall coefficient. The temperature-dependent in-plane resistivity at different dopings has been studied [15]. The temperature- and doping-dependent resistivity data are consistent with published data [16]. The critical temperature T_C has been determined from the temperature where the resistivity goes to zero at zero applied magnetic field. The resistive superconducting transition temperature T_C shows the same domelike behavior as published earlier [16]. LCCO shows very similar transport behavior as PCCO [17], but the superconducting dome is slightly shifted towards lower Ce concentration for LCCO. To understand the normal-state behavior the resistivity has been measured for *c*-axis magnetic field $H > H_{C2}$ [15]. The resistivity shows a low-T upturn for doping $x = 0.08$, 0.11, and 0.13, but, for $x > 0.14$ no upturn is observed. The temperature-dependent normal-state Hall coefficient (R_H) of LCCO films measured at 14 T magnetic field shows that R_H gradually changes from negative to positive value with increasing Ce concentration. R_H is negative for the samples $0.08 \leqslant x \leqslant 0.13$ and positive for $x \geqslant 0.14$, which confirms that a Fermi surface reconstruction occurs at $x = 0.14$ [15].

B. Vortex lattice melting in LCCO

In many conventional and nonconventional superconductors a vortex liquid state is a region in the H-T plane which results from the melting of the vortex solid above some characteristic magnetic field, H_{VS}, as a consequence of thermodynamic fluctuation of the superconducting order parameter [18]. In cuprate superconductors the vortex liquid phase exists between a vortex solid phase below $H_{VS}(T)$ and the normal state above $H_{C2}(T)$ due to a strong 2D character and a low superfluid density [19].

We have measured the in-plane electrical resistivity versus magnetic field up to 14 T at different temperatures below T_C for our LCCO films. H_{VS} has been taken as the critical magnetic field (at different temperatures and doping) where the resistance becomes nonzero. As an example, Fig. 1 shows a plot of the resistive transition versus field for $x = 0.15$ at different temperatures from 1.8 to 20 K. Previously it has been established in some hole-doped cuprates and the electron-doped PCCO [12] that there is no vortex liquid state at $T = 0$. Grissonnanche *et al.* have shown that $H_{C2} = H_{VS}$ at $T = 0$ in the hole-doped cuprates YBCO ($YBa_2Cu_3O_y$) and Y124 ($YBa_2Cu_4O_8$) from thermal conductivity measurements [20]. An expression for the vortex melting line due to thermal fluctuation has been derived using a nonlocal elasticity theory
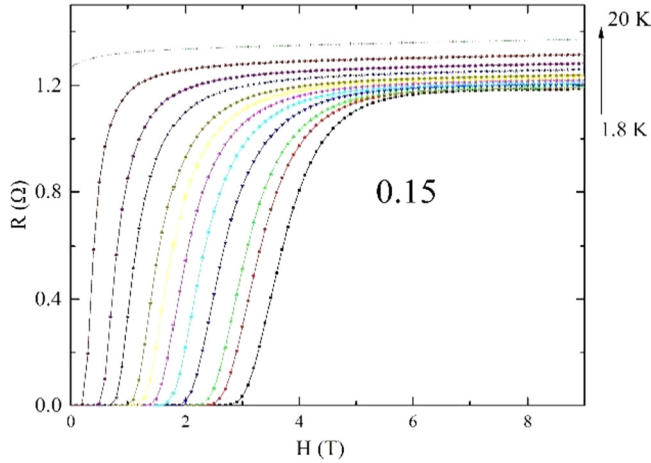
FIG. 1. The resistance of LCCO films for $x = 0.15$ as a function of magnetic field, from 1.8 to 20 K. The onset of resistivity as the magnetic field is increased marks the vortex lattice melting transition, $H_{VS}(T)$.

and Lindemann criteria by Houghton *et al.* for temperature dependence of H_{VS} [21]:

$$\frac{\sqrt{b_m(t)}}{1 - b_m(t)} \frac{t}{\sqrt{1-t}} \left[\frac{4\left(\sqrt{2} - 1\right)}{\sqrt{1 - b_m(t)}} + 1 \right] = \frac{2\pi c_L^2}{\sqrt{G_i}}, \quad (1)$$

where $t = T/T_C$, reduced field $b_m = H_{VS}(T)/H_{VS}(0)$, G_i is the Ginzburg number, and c_L is the Lindemann number. We have used the definitions of $G_i c_L$ as used by Ramshaw *et al.* [22]. Figure 2 demonstrates the resulting field-temperature phase diagram for a typical Ce concentration, $x = 0.14$. $H_{VS}(T)$ is extrapolated to $T = 0$ to get $H_{VS}(0)$ in the $T = 0$ limit. The black line is a fit to Eq. (1). The fitting of the data allows us to obtain the value of $H_{VS}(0)$ for different
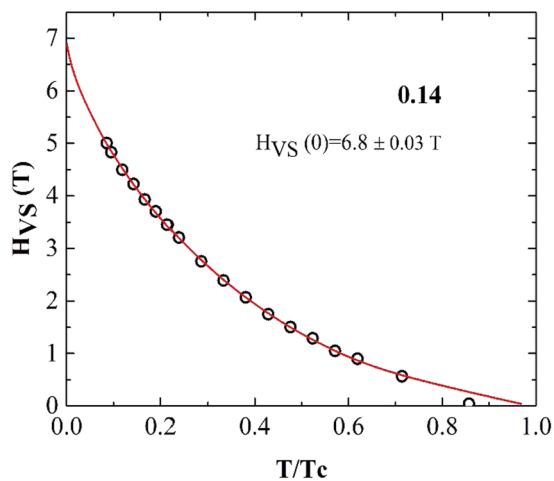

FIG. 2. The vortex solid melting transition as a function of temperature for $x = 0.14$. The temperature axis is scaled by T_C. The solid line is the best-fit line to Eq. (1); i.e., in text $H_{VS}(0)$ is obtained from the extrapolation of the best-fit line of $H_{VS}(T)$ to $T = 0$.

doping concentrations of Ce. We have plotted $H_{VS}(0)$ versus Ce doping in Fig. 12.

C. Vortex Nernst effect in LCCO

The vortex Nernst signal is defined as the transverse electric field generated by the vortices moving within the superconductor under the longitudinal thermal gradient and perpendicular magnetic field [23]. The vortex induced Nernst signal is well known from previous studies for conventional and high-T_C superconductors [1,23,24].

Figure 3 illustrates the typical magnetic field-dependent Nernst signal, $N = E_y/(-\nabla T)$ at different temperatures for the typical Ce doping (0.11) and (0.14) of LCCO thin films below T_C. The vortex induced Nernst signal peaks at a field H^*. The position of H^* shifts to the higher magnetic field with decreasing temperature, which follows the same behavior as the upper critical field H_{C2} in the superconducting state below T_C. Above H_{C2} the quasiparticle (normal-state) Nernst signal is nearly linear in field but with a small additional H^3 term [17]. The normal-state Nernst signal at higher field is subtracted from the measured data to obtain the net vortex signal as shown in the inset of Fig. 3 for $x = 0.14$ at 20.7 K. We will discuss the quasiparticle Nernst signal later.

D. Nernst effect in LCCO above T_C

The nature of the Nernst signal observed just above the transition temperature T_C is different from the Nernst signal well above T_C, i.e., in the normal state. Figure 4(a) shows the raw Nernst signal as a function of field at $T = 17.8$ K ($T > T_C = 15$ K) for $x = 0.15$ (overdoped). The Nernst signal increases initially at low field with a subsequent fall at higher field. After a certain field the signal again is observed to increase with further increase in magnetic field. The signal at the higher magnetic field is attributed to the background signal from a sizable contribution of the normal-state quasiparticles, which in general cannot be assumed to be negligible.

Therefore the total Nernst signal is the sum of the Nernst signal, N_{SC}, due to superconducting fluctuations and N_{qp} due to the quasiparticle contribution: $N = N_{SC} + N_{qp}$. We can estimate N_{qp} from the total Nernst signal N at an applied magnetic field $H > H_{C2}$. To estimate N_{qp} we have fitted the data above 10 T by using the power law: $N_{qp} = c_1(T)H + c_3(T)H^3$. The same fitting procedure has been applied to the Nernst data for other underdoped, optimally doped, and overdoped samples with slightly different values of c_1 and c_3 [17]. The dotted line is the fit of the high-field segments of the above-mentioned power law as shown in Fig. 4(a). Thus we can extract the contribution due to superconducting fluctuation by $N_{SC} = N - N_{qp}$. Figure 4(b) shows the superconducting signal N_{SC} as a function of magnetic field at the temperature of 17.8 K. The superconducting Nernst signal is observed to increase sharply at low magnetic field, reaches a maximum field H^*, and then decreases gradually to a weakly temperature-dependent magnitude. At high magnetic field N_{SC} is vanishingly small.

Figure 5 presents the raw Nernst isotherm at different temperatures above T_C for the typical concentration of Ce
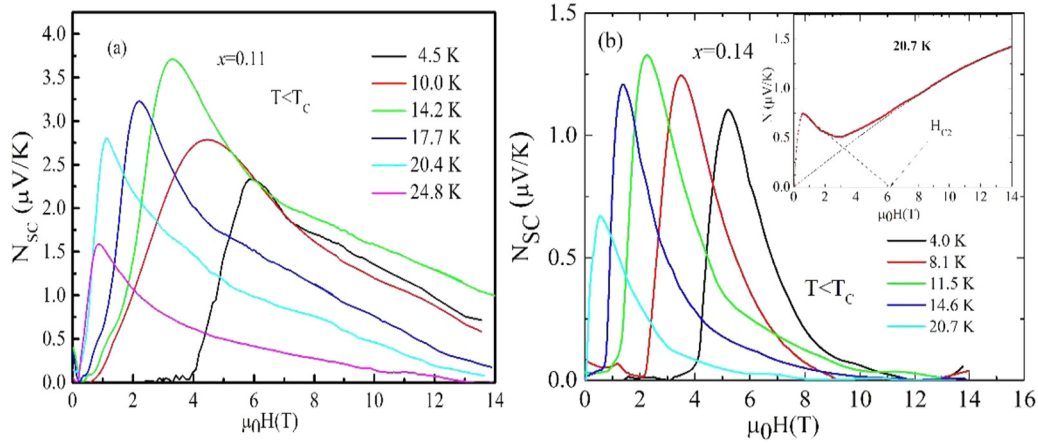
FIG. 3. (a) The superconducting Nernst signal N_{SC} of LCCO as a function of magnetic field below T_C for $x = 0.11$ and 0.14 with $T_C = 26$ and 21 K, respectively as determined by the onset of the resistive transition. The peak field, where the maximum of N_{SC} is obtained with quasiparticle background subtracted. Inset shows a typical raw Nernst signal N versus magnetic field H. The black dotted line represents the polynomial fit using the power law $N_{qp} = c_1(T)H + c_3(T)H^3$, where N_{qp} is the quasiparticle background. (b) N_{SC} of LCCO as a function of magnetic field below T_C for $x = 0.11$ with $T_C = 26$ K.

concentration, $x = 0.14$. For all the LCCO samples the superconducting Nernst signal shows the same behavior. Figure 6 shows the superconducting Nernst signal N_{SC} as a function of field at different temperatures for underdoped ($x = 0.08$), optimally doped ($x = 0.11$), and overdoped ($x = 0.13, 0.14$, and 0.16) samples. N_{SC} is observed to decrease with increase in temperature above T_C for all samples. There is no obvious change at the FSR doping. In contrast to the vortex peak in the superconducting state, the peak field H^* shifts to the higher fields with increase in temperature, which indicates fundamentally distinct origins of Nernst signal above and below the transition temperature. H^* is a characteristic field that was first identified by Kapitulnik *et al.* in disordered superconducting films of InGe [25]. Basically $H^*(T)$ (above T_C) mirrors the upper critical field $H_{C2}(T)$ (below T_C). For this reason these authors nicknamed it as the "ghost critical field." The ghost critical field is defined as the magnetic field scale above which the superconducting fluctuations are suppressed. Figure 7 shows H^* (obtained from the N_{SC} versus H plot) as a function of reduced temperature ε for all the samples. H^*

obeys the logarithmic dependence

$$H^* = H_{C2}^* \ln(T/T_C), \qquad (2)$$

where H_{C2}^* is an empirical parameter that characterizes the strength of the superconductivity [5].

To analyze the superconducting fluctuation deep inside the normal state above the transition temperature the Nernst effect is a powerful tool. A large Nernst signal has been detected in a broad interval above T_C in many hole-doped cuprates by the Princeton group in the period of 2000–2006 [1]. In the underdoped region the Nernst signal has been attributed to the superconducting phase fluctuation detectable up to $\sim 5T_C$. They have defined the extended region having a large signal above the "T_C dome" as the Nernst region. The electron-doped cuprate superconductors provide the interesting counterexample to the hole-doped cuprates. We have examined the Nernst region for electron-doped LCCO films for the underdoped, optimally doped, and overdoped samples. The upper limit of the Nernst region is defined as T_{onset}. In other words T_{onset} is defined as the temperature below which $\nu(T)/T$ starts to rise
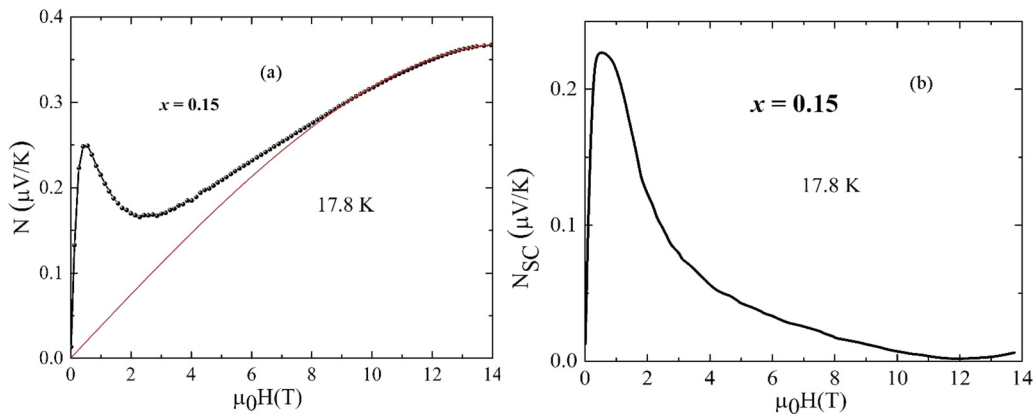

FIG. 4. (a) Raw Nernst signal N as a function of field H for $x = 0.15$ at $T = 17.8$ K. The red line is the polynomial fit to the raw data above 10 T, of the form $N_{qp} = c_1(T)H + c_3(T)H^3$. (b) Superconducting contribution to the Nernst signal as obtained by subtracting the normal-state quasiparticle Nernst signal N_{qp} from the raw Nernst response for $x = 0.15$. H^* represents the peak field in N_{SC} versus H plot above T_C.
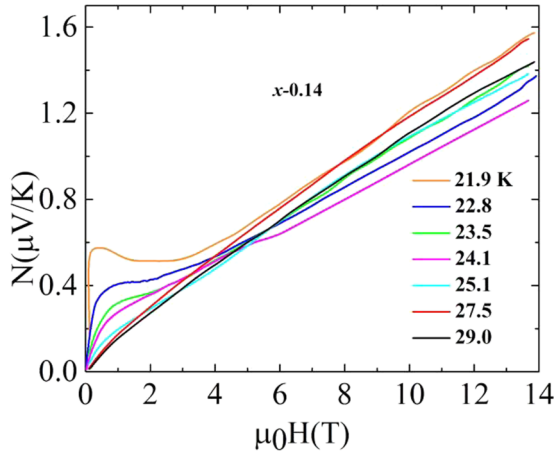
FIG. 5. Raw Nernst data as a function of field for $x = 0.14$ at different temperatures above T_C.

upon cooling. For example, the data of LCCO for $x = 0.08$ yield $T_{onset} \cong 34.2$ K as shown in Fig. 8. The phase diagram of T_{onset} versus x has been demonstrated in Fig. 9. T_{onset} exactly follows the T_C-like dome. The phase diagram demonstrates the continuity of the region up to which the Nernst signal due to superconducting fluctuation is observed above the T_C dome for each doping.

IV. DISCUSSION

In this section we will discuss the nature of the superconducting fluctuations in LCCO films. In addition the value of the upper critical field obtained from the Nernst data will be compared with the critical field obtained in the dirty limit from high-field transport properties. We also have determined the value of coherence length and the pairing gap in the LCCO thin films.

A. Superconducting fluctuations

The study of superconducting fluctuations had a remarkable revival after the discovery of the cuprate superconductors. Superconducting fluctuation can extensively be studied by the measurements of electrical resistivity, magnetization, and Nernst effect. The Nernst effect is a very sensitive probe to measure the superconducting fluctuation whereas it is very difficult to detect the superconducting fluctuation from the resistivity data. To understand the superconducting fluctuation and the strength of the superconductivity in electron-doped LCCO samples we have analyzed the data obtained from Nernst measurements.

To treat the fluctuation of the superconducting order parameter in the Gaussian approximation, the off-diagonal Peltier coefficient α_{xy} is an important thermodynamic-state function [11]. In the zero field limit α_{xy}/H is simply related to the Nernst coefficient ν and the electrical conductivity σ_{xx} of the sample through the formula $\alpha_{xy}/H \approx \nu \sigma_{xx}$, when the Hall conductivity is small. Normally in cuprates the transverse Hall conductivity is very small [26,12]. In superconductors, above the transition temperature the conductivity varies weakly with the change of the temperature and magnetic field. Therefore the Peltier coefficient is mostly governed by the magnitude of the Nernst coefficient. We have plotted the Nernst coefficient ν ($\nu = N/H$) versus magnetic field for the optimally doped sample ($x = 0.11$) at different temperatures above T_C as shown
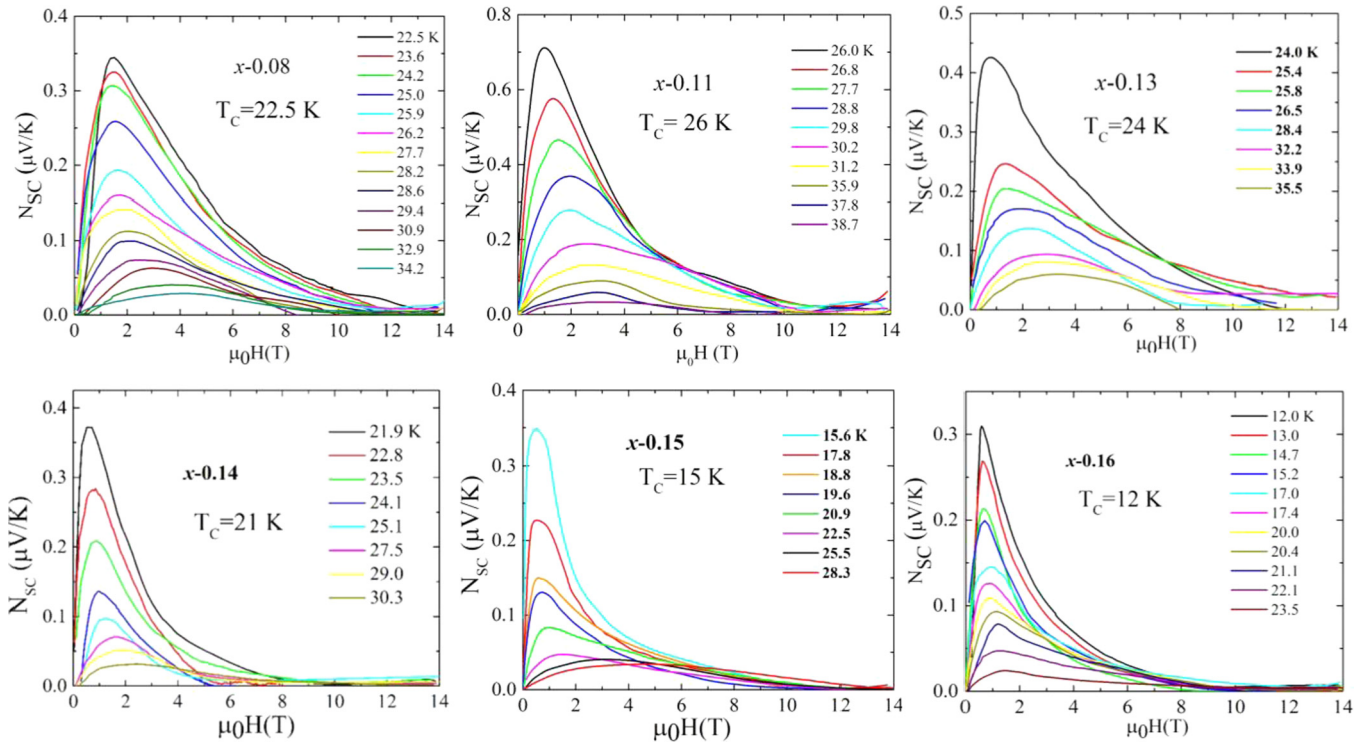

FIG. 6. Superconducting contribution to the Nernst signal at different temperatures above T_C for all doping. The peak field shifts towards higher field with increasing temperature.
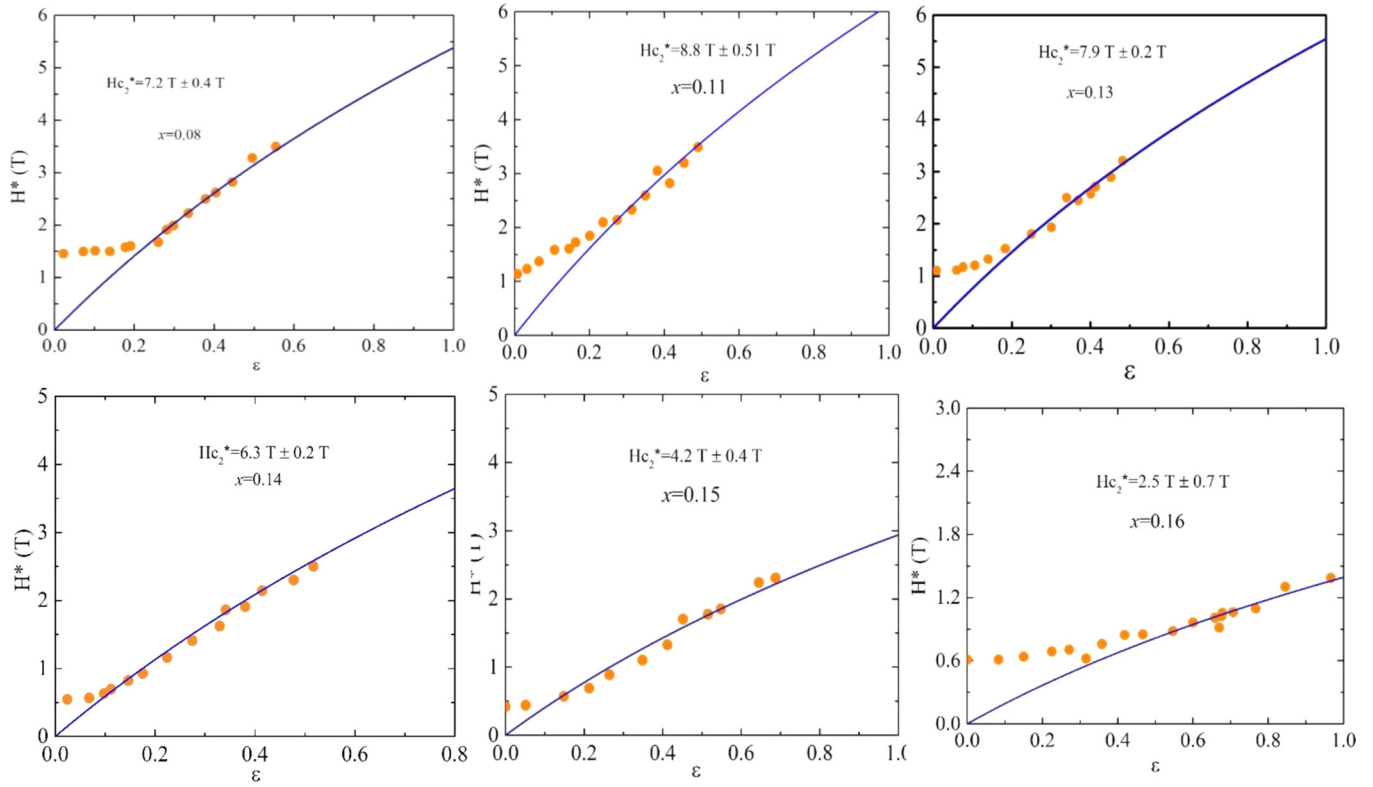
FIG. 7. The field scale H^* as a function of reduced temperature $\varepsilon = (T - T_C)/T_C$ in LCCO at doping as indicated. The solid lines are the fit to the function of logarithmic dependence $H^* = H^*_{C2} \ln(T/T_C)$. We can extract the characteristic field H^*_{C2} from the fittings for the samples.

in Fig. 10(a). We can see that ν is independent of magnetic field and is nearly constant in low magnetic field limit. From ν ($\nu = N/H$) versus H plots for all the samples the value of ν (ν_0) in the zero magnetic field limit has been extracted and plotted as the function of reduced temperature ε. The plot of ν_0 as a function of ε is shown in Fig. 10(b) for $x = 0.11$. To estimate the normal-state contribution, ν_0^{qp}, in the limit $H \to 0$ we have fitted the data and extracted the superconducting

contribution, $\nu_0^{sc} = \nu_0 - \nu_0^{qp}$ by using the power law: $\nu_0^{qp} = A(T)\, T + B(T)\, T^2$, where A and B are constants [5]. The same fitting procedure has been applied to the Nernst data for other underdoped, optimally doped, and overdoped samples with slightly different values of A and B. The solid black line as demonstrated in Fig. 10(b) represents the quasiparticle background to the Nernst coefficient. In Fig. 10(c) we have displayed the superconducting contribution to ν_0 called ν_0^{sc} versus reduced temperature for $x = 0.11$ after subtracting the quasiparticle contribution ν_0^{qp}.
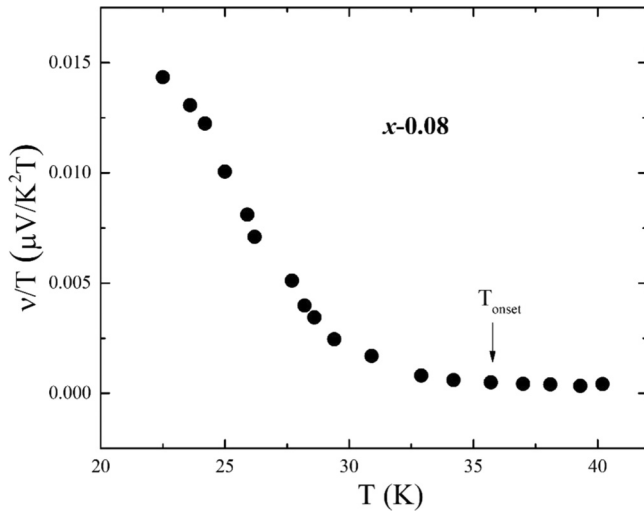

FIG. 8. Nernst coefficient ν of LCCO at the electron doping $x = 0.08$, plotted as ν/T versus temperature T at a magnetic field of 2 T. The onset temperature T_{onset} is indicated by the arrow.
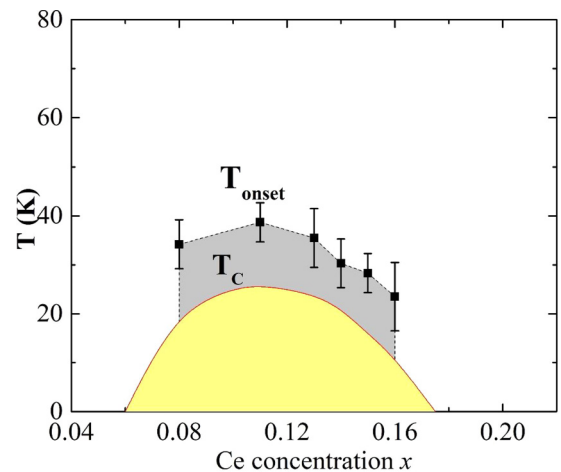

FIG. 9. The phase diagram of LCCO showing the SC fluctuation Nernst region between the T_C dome and T_{onset} based on Nernst measurements for six different dopings. T_{onset} tracks the T_C dome.
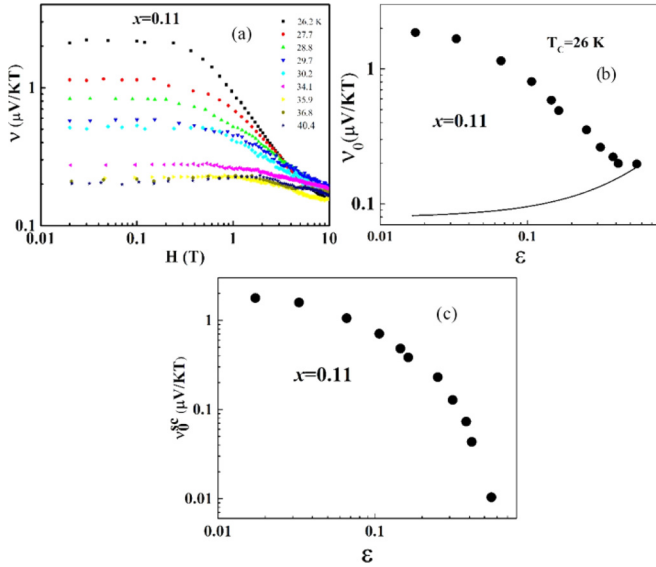
FIG. 10. (a) Nernst coefficient as a function of magnetic field for the optimally doped sample (Ce = 0.11) measured at temperature exceeding T_C. As $H \to 0$, the Nernst coefficient is independent of magnetic field with a constant value ν_0. At higher magnetic field the Nernst coefficient becomes independent of temperature. (b) ν_0 as a function of reduced temperature ε for $x = 0.11$. The solid line is the normal-state contribution (ν_{qp}) to ν_0. (c) ν_0^{SC} (obtained by subtracting the ν_{qp} from the Nernst coefficient ν_0) as a function of reduced temperature ε for $x = 0.11$.

B. Comparison to temperature-dependent Gaussian theory

We have calculated the contribution of Gaussian superconducting fluctuations to the transverse thermoelectric response above T_C in the low magnetic field limit. However, it should be emphasized that the temperature up to which the fluctuation can be detected is a question of sensitivity and signal-to-background ratio. In this study we have tracked the fluctuations up to $\sim 1.6 T_C$ for LCCO thin films. The value of α_{xy}^{SC} has been determined experimentally using the equation

$$\frac{\alpha_{xy}^{SC}}{H} \approx \frac{\nu_0^{SC}}{\rho_s}, \tag{3}$$

where the superconducting Nernst coefficient $\nu_0^{SC} = \nu_0 - \nu_0^{qp}$ in the zero field limit and $\rho_s = \rho/s$; s is the interlayer separation (6.1 Å). Figure 10(c) displays ν_0^{SC} as a function of reduced temperature ε for $x = 0.11$.

Superconductivity is normally characterized by the superconducting order parameter SOP ($|\Psi|e^{i\theta}$) which comprises the amplitude Ψ and the phase θ at each space point [27]. Fluctuation in either amplitude or phase or both amplitude and phase can affect the superconducting properties and the Nernst signal can be enhanced [28]. Superconducting fluctuations deal with the thermal fluctuations of the SOP [29]. By using the time-dependent Ginzburg-Landau equation in the Gaussian approximation, Ussishkin et al. calculated the off-diagonal component of the Peltier conductivity tensor, α_{xy}, which results from the contribution of Gaussian superconducting fluctuations to thermoelectricity [2]. The value of α_{xy}^{SC}/H is independent of magnetic field at low magnetic field. In

2009, Serbyn et al. [30] and Michaeli and Finkel'stein [11] calculated α_{xy}^{SC} for 2D type-II dirty s-wave superconductor independently up to arbitrary T and arbitrary H. In 2012 and 2014, calculation of α_{xy}^{SC} was performed for hole-doped Eu-LSCO and electron-doped PCCO, respectively [5,12].

We have compared the temperature dependence of α_{xy}^{SC} measured for our LCCO thin films with the predictions of Gaussian theory in the low-field limit ($H \to 0$). In the low-field limit, the Aslamazov-Larkin theory of superconducting fluctuation predicts that

$$\frac{\alpha_{SC}^{xy}}{H} = \nu_{SC}\sigma_{xx} \sim \frac{\xi_0^2}{T \ln(T/T_C)}, \tag{4}$$

where ξ_0 is the Ginzburg-Landau coherence length at zero temperature. Therefore, for a given T, α_{SC}^{xy} depends only on one quantity ξ_0. The extracted values of $\frac{\alpha_{SC}^{xy}}{H}$ at zero magnetic field are shown in Fig. 11 for $x = 0.08$, 0.11, and 0.14. As shown in Fig. 11 the data are observed to follow the theoretical temperature dependence for underdoped, optimally doped, and overdoped samples. The agreement between theoretical and experimental data is excellent. It is evident from Fig. 11 that the Gaussian theory can reliably explain the superconducting fluctuation from the underdoped to the overdoped regime.

C. H_{C2} (0) and H_{C2}^*

The doping dependence of H_{C2} has been reported for hole-doped and electron-doped cuprates using high-field measurements of H_{VS} (T). For TI-2201 (Tl$_2$Ba$_2$CuO$_{6+\delta}$) and YBCO it has been shown that the H_{VS} (0) extrapolated from the resistive H_{VS} (T) is consistent with the H_{C2} (0) value obtained from a low-temperature thermal conductivity measurement [20]. The field-temperature phase diagram for both YBCO and Y124 (YBa$_2$Cu$_4$O$_8$) demonstrates that H_{C2} (T) and H_{VS} (T) converge at $T = 0$ K, where H_{VS} (T) is obtained from high-field resistivity data and H_{C2} (T) has been determined from the thermal conductivity measurement. Therefore from those measurements of H_{VS} versus T one can determine H_{C2} (0). The data H_{C2} (0) = H_{VS} (0) have also been confirmed for the electron-doped PCCO at $x = 0.15$ [12]. Based on these prior investigations we take H_{VS} (0) as H_{C2} (0) in the present study.

We have compared the critical field in the LCCO films in two different ways: (a) from high-field transport measurements below T_C, denoted as H_{C2} (0) as discussed above and (b) H_{C2}^* directly obtained from the Nernst data above T_C. The two measured values of critical field are in reasonable agreement. Both have their highest value near optimal doping. With increasing doping the magnitude is observed to decrease and in the case of the underdoped sample the value of the upper critical field is also lower than the optimally doped one as shown in Fig. 12.

The variation of H_{C2}^* has been displayed in Fig. 12. To determine H_{C2}^*, the ghost critical field H^* has been plotted versus reduced temperature $\varepsilon = (T - T_C)/T_C$ for the samples as shown in Fig. 10. H^* obeys Eq. (2) for all the samples up to high temperature, namely, the reduced temperature of $\varepsilon \approx 0.6$. Below $\varepsilon \approx 0.15$ H^* deviates from the relation of Eq. (2). This deviation has been attributed to the divergence of paraconductivity in the $\varepsilon \to 0$ limit [2]. The Nernst signal
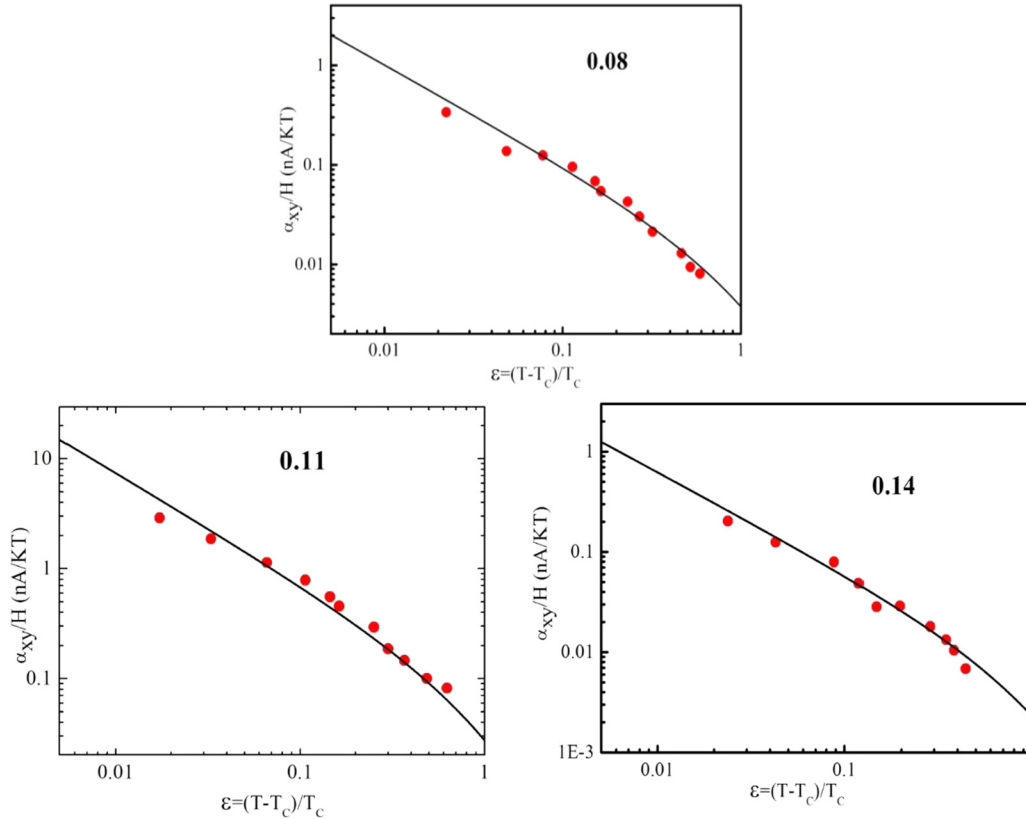
FIG. 11. $\alpha_{xy}/H = \nu/\rho_{xx}$ in the zero field limit extracted from the measured Nernst coefficient and resistivity in LCCO for $x = 0.08$, 0.11, and 0.14. The solid line is the theoretical expectation for the zero field limit from Gaussian fluctuations.

N_{SC} is the ratio of the off-diagonal Peltier coefficient (α_{xy}) from superconductivity fluctuation to the electrical conductivity (σ_{xx}). In the $\varepsilon \to 0$ limit both α_{xy} and σ_{xx} diverge [2]. Using Eq. (2) the values of H_{C2}^* have been determined for the underdoped, optimally doped, and overdoped samples. These values can be compared with the estimated upper critical field $H_{C2}(0)$, which has been obtained as the resistive critical field $H_{VS}(0)$ as shown in Fig. 2. The value of H_{C2}^* extracted from the fit for each doping has been plotted in Fig. 12. The main finding is that the field scale of the superconductivity decreases with

FIG. 12. The phase diagram of two magnetic field scales of the superconductivity in LCCO plotted as a function of Ce doping.

decreasing doping with a local maximum at optimal doping and again decreases with increase above optimal doping. The obtained result is free from any theory or model and can be directly read off from the raw isothermal Nernst data as a function of magnetic field. $H_{VS}(0)$ has been observed to be higher than the upper critical field H_{C2}^* for optimally ($x = 0.15$) doped $Pr_{2-x}Ce_xCuO_4$ (PCCO) [12]. The anomaly in $H_{VS}(0)$ seen in PCCO has been linked to the Fermi surface reconstruction (FSR) ($x = 0.16$). A similar trend of $H_{VS}(0)$ is observed near optimally doped LCCO ($x = 0.11$) as reported in our paper. However, the Fermi surface reconstruction in LCCO is at $x = 0.14$, which is much higher than the optimally doped LCCO where $H_{VS}(0)$ follows H_{C2}^*. From our finding it is not possible to link the FSR to the cause of the $H_{VS}(0)$ anomaly. It is not clear that why the values are different near an optimally electron-doped superconductor. However, $H_{VS}(0)$ and H_{C2}^* closely track the superconducting dome.
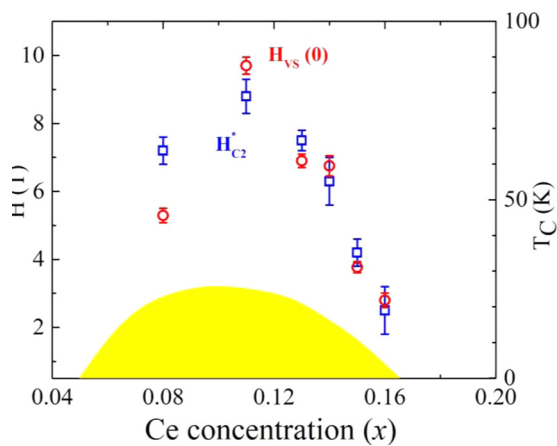
D. Determination of ξ_0 and Δ_0

We carried out the scaling comparison for the over-doped, optimal-doped and under-doped samples of LCCO films. In type-II superconductors the upper critical field H_{C2} is an important parameter which determines the pairing gap Δ_0 through the coherence length ξ_0, i.e., the size of the Cooper pair and the strength of the Cooper pairing potential [9]. The pairing potential is stronger and the pair size is smaller for higher H_{C2}. Below H_{C2} the vortex liquid state appears in the sample. But the vortex liquid immediately forms a lattice and thus the electrical

resistance is going to be zero and the vortex melting field H_{VS} is equal to H_{C2}. In cuprate superconductors the vortex liquid phase intervenes between the vortex solid phase and the normal state. The value of the pairing gap is a polarizing issue for understanding the strength of the superconductivity in cuprates. So far, different evolution of pairing gap and the estimation of upper critical field H_{C2} are in sharp contradiction [5,31].

According to the BCS theory the energy gap to the onset of single-particle excitations decreases from a certain value at $T = 0$ K to zero at $T = T_C$ [32]. In the case of a d-wave superconductor the gap according to BCS is $\Delta_0 = 2.14 k_B T_C$ [33]. The behavior of the gap amplitude for all doping of LCCO is shown in Fig. 13. Just like $Pr_{2-x}Ce_xCuO_{4-\delta}$ the superconducting gap follows the doping dependence of T_C [34]. The behavior of H_{C2}^* in our experiment is consistent with the behavior of the gap amplitude at different Ce doping as shown in Figs. 12 and 13.

Now we will discuss the determination of the coherence length ξ_0 for different dopings directly using the value of H_{C2}^*. In the case of cuprate superconductors the strongly correlated background is weakened by increased doping. The behavior of various superconductivity characteristics, superconducting fluctuation, and their predominance in the phase diagram depend on different material-dependent parameters like quenched disorder, dimensionality, or the superconducting coherence length, etc. [35]. The upper critical field is closely related to the superconducting gap magnitude Δ_0. The upper critical field and the superconducting gap can be compared directly by converting them to the length scales. The gap amplitude can be converted to the Pippard coherence length by

$$\xi_p = \hbar v_F / a \Delta_0, \qquad (5)$$

where v_F (2.9×10^5 m/s), for the overdoped n-type cuprate NCCO [36], is the Fermi velocity; $a = 1.5$ (for d-wave superconductor); and Δ_0 is the superconducting gap amplitude. The value of the Fermi velocity has been determined from the quantum oscillation measurements. Δ_0 is $2.14 k_B T_C$ for a d-wave state. In a dirty superconductor the Pippard's relation for the coherence length is

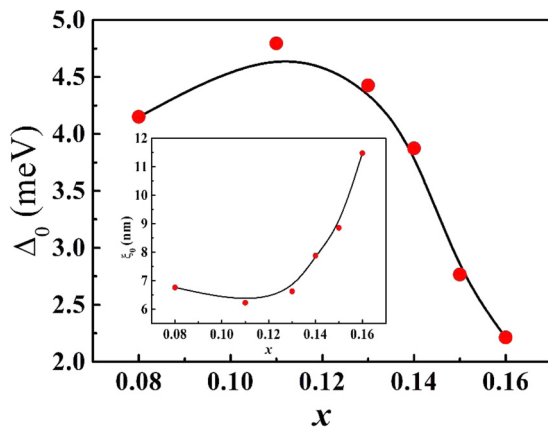$$\frac{1}{\xi_0^{dirty}} = \frac{1}{\xi_p} + \frac{1}{l}, \qquad (6)$$

FIG. 13. Ce dependence of superconducting gap. Inset shows the coherence length obtained from H_{C2}^*.

where l ($l = hs/e^2\rho_0 k_F$) is the mean free path, s (6.1 Å) is the interlayer distance, k_F (0.58 Å^{-1}) is the Fermi wave vector, and ξ_0^{dirty} is the coherence length at $T = 0$. $\rho_0 = 17\,\mu\Omega$ cm is the residual resistivity for $x = 0.16$. We get the value of ξ_0 as 12.5 nm which is consistent with the previous results in the overdoped PCCO, $x = 0.17$ (ξ_0 was calculated to be 10.9 nm) [13]. We can estimate the value of the upper critical field by using the value of the coherence length in the dirty limit,

$$H_{C2} = \varphi_0 / 2\pi \left(\xi_0^{dirty} \right)^2. \qquad (7)$$

H_{C2} is calculated to be 2.1 T for the 0.16 sample. For overdoped PCCO, H_{C2} was observed to be 3.7 T [13]. We get the upper critical field of 2.5 T from Nernst measurement and H_{VS} (0) of 2.8 T from high-field magnetoresistance measurement for $x = 0.16$. Therefore we can see that the value of the upper critical field obtained from fluctuation above T_C is in good agreement with the critical field expected for the sample in the dirty limit and the high-field transport directly measured at $T < T_C$.

According to Pourret et al. at a temperature above T_C for the conventional superconductor $Nb_{0.15}Si_{0.85}$ there is a magnetic field called the ghost critical field below which the superconducting fluctuation is controlled by the coherence length $\xi (T) = \xi (0)/[\ln(T/T_C)]^{1/2}$ and above which its extent is controlled by the magnetic length $l_B = (\hbar/2eB)^{1/2}$ [9]. At the ghost critical field the two length scales become the same, i.e., $\xi (H^*) = l_B (H^*)$, i.e., $H^* = (\varphi_0/2\pi\xi_0^2)\ln(T/T_C)$, where the flux quantum $\varphi_0 = h/2e$ and $H_{C2} (0) = (\varphi_0/2\pi\xi_0^2)$. As we have discussed, $H_{C2} (0)$ is nearly equal to H_{C2}^*, so we can roughly estimate the value of the coherence length ξ_0 from $H_{C2}^* = (\varphi_0/2\pi\xi_0^2)$. We thus can determine the value of the coherence length ξ_0 for different dopings directly using the value of H_{C2}^*. The inset of Fig. 13 displays the coherence length at different doping concentrations. From the calculated value of H_{C2}^* and ξ_0 we can say that the strength of the superconductivity develops and the coherence length vanishes simultaneously.

The present experiment establishes that the upper critical field increases as Ce doping decreases, is highest for the optimally doped sample, and again decreases for the underdoped sample, which implies that the superconductivity is strongest for the optimally doped sample. The trend of Δ_0 suggests the dome shape of the entire cuprate phase diagram.

E. Possible origin of the T_C dome

We attribute the weakening of the strength of the superconductivity and the fall of the transition temperature T_C with underdoping as coming from competition with the onset of antiferromagnetic order. Very few experiments have been performed in $La_{2-x}Ce_xCuO_4$ because it can only be made in a thin-film form and no crystals can be prepared. Therefore neutron scattering, NMR (Nuclear magnetic resonance), and bulk μSR (Muon spin spectroscopy) are not possible for a study of the magnetism of LCCO. Recently from a depth resolved low-energy μSR study of $La_{2-x}Ce_xCuO_4$ films the presence of long-range antiferromagnetic (AFM) order has been observed up to just below optimal doping [37]. The static three-dimensional (3D) magnetism (e.g., long-range antiferromagnetism) is absent in the $x = 0.10$ sample, but

present in $x = 0.07$ below 65 K and $x = 0.08$ below 40 K. Above $x = 0.10$ there is short-range AFM order. The transition of long-range antiferromagnetic order to short-range antiferromagnetic order is also observed for NCCO from inelastic neutron scattering measurements [38]. Thus the competition with the long-range AFM order weakens the superconductivity and both H_{C2} and T_C fall in the underdoped La$_{2-x}$Ce$_x$CuO$_4$.

F. T_{onset}

In hole-doped cuprates the Nernst results suggested that above T_C superconductivity disappears because of the loss of long-range phase coherence [1]. At a temperature called T_{onset} the Nernst region in these cuprates does not extend to the pseudogap temperature T^* but lies between T_C and T^* for underdoped samples. For underdoped samples T_{onset} falls steeply when x tends to zero, whereas T^* is observed to increase continuously. Below T_{onset} the presence of the Nernst signal and the diamagnetic response are distinct signatures of fluctuating superconductivity [1]. For electron-doped cuprates a pseudogap phase has not been observed; only a region of AFM fluctuations above T_C is observed. In the superconducting dome all the LCCO films exhibit a fluctuation Nernst signal above T_C up to a characteristic crossover temperature T_{onset} as shown in Fig. 9. For LCCO thin films the optimally doped ($x = 0.11$) sample has the highest temperature range and thus T_{onset} ($\cong 39$ K) is high for $x = 0.11$. For higher doping T_{onset} decreases and tends to zero along with the critical temperature at the end of the superconducting dome. Both T_{onset} and H_{C2} are observed to track the T_C dome in LCCO. It seems that, over the broad interval $T_{\text{onset}} > T > T_C$, the superconducting pairing strength and the superconducting fluctuation may be intimately related. Similarly in hole-doped LSCO the Nernst region has been observed to be diminished at the end of the superconducting dome [1] implying that there is a common relation between superconducting fluctuation and pairing in both electron- and hole-doped cuprates.

V. SUMMARY AND CONCLUSION

We have performed measurements of the Nernst effect in electron-doped La$_{2-x}$Ce$_x$CuO$_4$ films over a wide range of doping and temperature above and below T_C. Above the superconducting transition temperature the field-dependent Nernst signal reveals a field scale that increases with increasing temperature. We have uncovered an extended region above the superconducting dome where the Nernst signal exists. The upper limit of the Nernst signal has been defined by T_{onset} which is high for optimally doped LCCO film. The Nernst signal above the critical temperature displays a smooth continuity with the vortex liquid melting field at zero temperature.

By subtracting the quasiparticle contributions to zero in the normal state of the LCCO films we have resolved a sizable Nernst signal coming from fluctuating Cooper pairs. We also have elucidated the nature of superconducting fluctuation from the Nernst measurements above critical temperature. A quantitative agreement with the theoretical prediction of Gaussian fluctuations in the zero field limit has been observed for all doping.

We have extracted the characteristic field H_{C2}^* directly from the measurements of the Nernst effect, which determines the value of coherence length, i.e., the size of the Cooper pair and the strength of pairing potential. The pairing potential is stronger and the pair size is smaller for optimally doped ($x = 0.11$) LCCO thin films. A domelike doping dependence of pairing potential, similar to the T_C dependence, is observed. The weakening of the pairing strength and the fall of the transition temperature T_C with underdoping has been attributed to the onset of antiferromagnetic order. Surprisingly, no special feature in the pairing potential occurs at the doping ($x = 0.14$) where the Fermi surface undergoes a reconstruction for LCCO films.

[1] Y. Wang, L. Li, and N. P. Ong, Phys. Rev. B **73**, 024510 (2006).

[2] I. Ussishkin, S. L. Sondhi, and D. A. Huse, Phys. Rev. Lett. **89**, 287001 (2002).

[3] L. Li, Y. Wang, S. Komiya, S. Ono, Y. Ando, G. D. Gu, and N. P. Ong, Phys. Rev. B **81**, 054510 (2010).

[4] I. Kokanović, D. J. Hills, M. L. Sutherland, R. Liang, and J. R. Cooper, Phys. Rev. B **88**, 060505(R) (2013).

[5] J. Chang, N. Doiron-Leyraud, O. Cyr-Choiniere, G. Grissonnanche, F. Laliberté, E. Hassinger, J.-P. Reid, R. Daou, S. Pyon, T. Takayama, H. Takagi, and L. Taillefer, Nat. Phys. **8**, 751 (2012).

[6] P. Li and R. L. Greene, Phys. Rev. B **76**, 174512 (2007).

[7] Y. Dagan, M. M. Qazilbash, C. P. Hill, V. N. Kulkarni, and R. L. Greene, Phys. Rev. Lett. **92**, 167001 (2004).

[8] Z. A. Xu, N. P. Ong, Y. Wang, T. Kakeshita, and S. Uchida, Nature **406**, 486 (2000).

[9] A. Pourret, H. Aubin, J. Lesueur, C. A. Marrache-Kikuchi, L. Bergé, L. Dumoulin, and K. Behnia, Nat. Phys. **2**, 683 (2006).

[10] A. Pourret, H. Aubin, J. Lesueur, C. A. Marrache-Kikuchi, L. Bergé, L. Dumoulin, and K. Behnia, Phys. Rev. B **76**, 214504 (2007).

[11] K. Michaeli and A. M. Finkel'stein, Europhys. Lett. **86**, 27007 (2009).

[12] F. F. Tafti, F. Laliberté, M. Dion, J. Gaudet, P. Fournier, and L. Taillefer, Phys. Rev. B **90**, 024519 (2014).

[13] H. Balci, C. P. Hill, M. M. Qazilbash, and R. L. Greene, Phys. Rev. B **68**, 054520 (2003).

[14] P. Fournier, X. Jiang, W. Jiang, S. N. Mao, T. Venkatesan, C. J. Lobb, and R. L. Greene, Phys. Rev. B **56**, 14149 (1997).

[15] T. Sarkar, P. R. Mandal, J. S. Higgins, Y. Zhao, H. Yu, K. Jin, and R. L. Greene, Phys. Rev. B **96**, 155449 (2017).

[16] K. Jin, N. P. Butch, K. Kirshenbaum, J. Paglione, and R. L. Greene, Nature **476**, 73 (2011).

[17] N. P. Armitage, P. Fournier, and R. L. Greene, Rev. Mod. Phys. **82**, 2421 (2010).

[18] D. S. Fisher, M. P. A. Fisher, and D. A. Huse, Phys. Rev. B **43**, 130 (1991).

[19] G. Blatter, M. Y. Feigel'man, Y. B. Geshkenbein, A. I. Larkin, and V. M. Vinokur, Rev. Mod. Phys. **66**, 1125 (1994).

[20] G. Grissonnanche, O. Cyr-Choiniére, F. Laliberté, S. René de Cotret, A. Juneau-Fecteau, S. Dufour-Beauséjour, M.-E. Delage, D. Le Boeuf, J. Chang, B. J. Ramshaw, D. A. Bonn, W. N. Hardy, R. Liang, S. Adachi, N. E. Hussey, B. Vignolle, C. Proust, M. Sutherland, S. Krämer, J.-H. Park *et al.*, Nat. Commun. **5**, 3280 (2014).

[21] A. Houghton, R. A. Pelcovits, and A. Sudbø, Phys. Rev. B **40**, 6763 (1989).

[22] B. J. Ramshaw, J. Day, B. Vignolle, D. LeBoeuf, P. Dosanjh, C. Proust, L. Taillefer, R. Liang, W. N. Hardy, and D. A. Bonn, Phys. Rev. B **86**, 174501 (2012).

[23] N. P. Ong, Y. Wang, S. Ono, Y. Ando, and S. Uchida, Ann. Phys. **13**, 9 (2004).

[24] K. Behnia, *Fundamentals of Thermoelectricity* (Oxford University Press, Oxford, 2015).

[25] A. Kapitulnik, A. Palevski, and G. Deutscher, J. Phys. C: Solid State Phys. **18**, 1305 (1985).

[26] K. Behnia and H. Aubin, Rep. Prog. Phys. **79**, 046502 (2016).

[27] M. Tinkham, *Introduction to Superconductivity*, 2nd ed. (McGraw-Hill, New York, 1996).

[28] V. J. Emery and S. A. Kivelson, Nature **374**, 434 (1995).

[29] A. I. Larkin and A. A. Varlamov, *The Physics of Superconductors*, Vol 1: Conventional and High-T_C Superconductors (Springer, Berlin, 2003).

[30] M. N. Serbyn, M. A. Skvortsov, A. A. Varlamov, and V. Galitski, Phys. Rev. Lett. **102**, 067001 (2009).

[31] Y. Wang, S. Ono, Y. Onose, G. Gu, Y. Ando, S. Tokura, S. Uchida, and N. P. Ong, Science **299**, 86 (2003).

[32] J. Bardeen, L. N. Cooper, and J. R. Schrieffer, Phys. Rev. **108**, 1175 (1957).

[33] M. Sutherland, D. G. Hawthorn, R. W. Hill, F. Ronning, H. Zhang, E. Boaknin, M. A. Tanatar, J. Paglione, R. Liang, D. A. Bonn, W. N. Hardy, and L. Taillefer, Phys. C (Amsterdam, Neth.) **408-410**, 672 (2004).

[34] I. Diamant, R. L. Greene, and Y. Dagan, Phys. C (Amsterdam, Neth.) **470**, S181 (2010).

[35] N. Kristoffel, T. Örd, and P. Rubin, Phys. C (Amsterdam, Neth.) **437-438**, 168 (2006).

[36] T. Helm, M. V. Kartsovnik, M. Bartkowiak, N. Bittner, M. Lambacher, A. Erb, J. Wosnitza, and R. Gross, Phys. Rev. Lett. **103**, 157002 (2009).

[37] H. Saadaoui, Z. Salman, H. Luetkens, T. Prokscha, A. Suter, W. A. MacFarlane, Y. Jiang, K. Jin, R. L. Greene, E. Morenzoni, and R. F. Kiefl, Nat. Commun. **6**, 6041 (2015).

[38] E. M. Motoyama, G. Yu, I. M. Vishik, O. P. Vajk, P. K. Mangand, and M. Greven, Nature **445**, 186 (2007).